Gait Development On A Direct Drive, Quadrupedal Robot

Daniel J. Blackman, John V. Nicholson, Camilo Ordonez, Bruce D. Miller, and Jonathan E. Clark

FAMU/FSU College of Engineering, 2003 Levy Drive, Tallahassee, FL 32310, USA

ABSTRACT

The development of dynamic, quadrupedal robots is becoming an increasing topic of interest with the growing demand for robotic interaction in the human environment, but they require adaptable control schemes to address the challenges encountered while traversing real world terrains. In this study, we explore improvements to both physical and control methods to a quadrupedal system in order to achieve fast, stable walking and trotting gaits. This analysis includes an investigation of physical compliance, 5-bar kinematics for trajectory shaping, and the implementation of ground and obstacle contact sensing. Structural and mechanical improvements were made to reduce undesired compliance to generate faster, more stable gaits. Contact sensing was implemented for identifying obstacles and deviations in surface level for negotiation of varying terrain. Overall, the incorporation of these features greatly enhances the mobility of the dynamic quadrupedal robot and helps to establish a basis for overcoming obstacles.

Keywords: gait development, quadrupedal locomotion, quadrupedal dynamics, terrain negotiation, obstacle detection, 5-bar kinematics

1. INTRODUCTION

Dynamic legged robotic systems have been shown to possess the ability to overcome a variety of terrains, making them a desirable avenue for developing robots that can interact more effectively with the human environment.[1–3] The complexity involved in designing and implementing dynamic gaits on multi-legged platforms has led to the establishment of a variety of methods for approaching this challenging issue.[4–7] An early and successful approach to gait development utilized clock-driven trajectories.[8,9] Other researchers have mimicked the kinematic motion primitives of animals such as horses.[10] Alternative biologically-inspired approaches include the development of complex neural networks and central pattern generators in order to establish more robust gaits.[11–14] Many of these more complex controllers require the incorporation of environmental sensory information, such as orientation awareness and obstacle detection. Though at times challenging to implement, controllers leveraging these sensing capabilities can adapt to difficult terrain such as sloped surfaces[15] or even stairs.[16]

In this paper we examine the application of a variety of these techniques on a new quadruped that implements a unique 5-bar kinematic leg design, Minitaur[17] (shown in Fig. 1). Minitaur's direct drive motors and 5-bar linkage leg design have several advantages. First, the direct drive system allows for the production of high frequency gaits. The leg configuration allows the motors to be located at the hip of the robot, thereby decreasing leg mass and reducing the inertial effects during these high speed motions. The high torque motors and 5-bar legs also reduce the necessity for a gear box by producing variable transmission rates, minimizing the reflected inertia. The hollow core motors used provide sufficient torque for developing running gaits, though low torque regions of the workspace can pose a challenge.[18]

This paper describes the development of gaits for Minitaur in order to exploit the unique kinematic properties of its direct drive leg design. Section 2 describes the development of a clock-driven gait inspired by previous success on robots such as Rhex[3] and iSprawl[19] whose controllers exist in the motor space. Section 3 highlights a series of mechanical modifications to improve the robot's physical robustness. Modifications made to the posture and to the shape of the leg trajectory to account for the effects of the mechanical modifications are given in Section 4. In Section 5, methods of foot sensing are explored in order to provide the framework for designing more robust gaits and incorporating obstacle detection. Some conclusions and avenues for future work are given in Section 6.

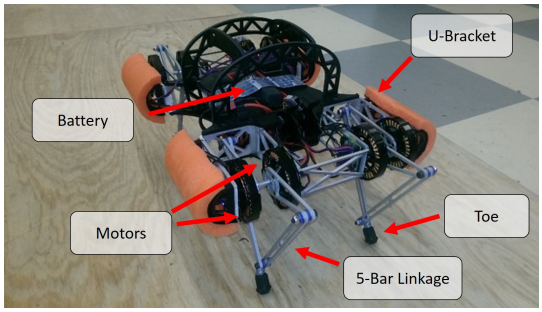

(a)

Minitaur Mechanical Parameters	
Parameter	Value
Mass	5.15 kg
Length	45.72 cm
Width	30.47 cm
Primary Link (L_1)	10 cm
Secondary Link (L_2)	20 cm
Toe Extension	2.5 cm

(b)

Figure 1: Minitaur is a dynamic quadruped designed using a direct drive 5-bar mechanism for its legs. This design involves the coaxial location of two motors separated by a space wide enough to contain the segments of the leg and allowing a large range of movement. (a) Minitaur with mechanical modifications to help protect its onboard electronics and minimize the impact of rolling. (b) Mechanical parameters of the robot previous to the structural modifications (of these parameters, only the mass was afflicted).

2. MOTOR SPACE GAIT DESIGN

Inspired by the success of early dynamic running by robots whose controllers exist in the motor space, we began with open loop trajectories formulated in referenced to the motor positions (θ_1 and θ_2 as defined in Fig. 2). Both the stance and flight phases of Minitaur's leg trajectories were implemented in the motor space and defined with respect to the desired orientation of the leg.

For the stance phase (which nominally begins at TD in Fig. 2), the motors begin with $\theta_1 = 90° + \psi_s/2$ and $\theta_2 = 90° - \psi_s/2$ with respect the vertical line. Then, both motors are rotated through the sweep angle (ψ_s) to the positions of $\theta_1 = 90° - \psi_s/2$ and $\theta_2 = 90° + \psi_s/2$, producing the base of the roughly triangular trajectory. The rate of rotation for stance was defined using the sweep angle ψ_s and the duty factor DF as follows:

$$R_1 = \frac{\psi_s}{DF} \tag{1}$$

At the apex of the flight phase, the toe is centered so that $\theta_1 = \theta_2$ and the foot is elevated to provide ground clearance. To accomplish this in the motor space, each motor was rotated at a different rate. To avoid reaching the singularity* of the 5-bar mechanism, a ground clearance factor (g_{cl}) was defined and tested using Matlab simulation to obtain a desired level of toe lift. For half of the remainder of the duty factor (DF), the motor defined by θ_1 rotated at the faster rate (3) while θ_2 rotated at the slower rate (2), both clockwise. This resulted in the overall centering and lifting of the toe.

$$R_2 = \frac{g_{cl}\psi_s}{1 - DF/2} \tag{2}$$

$$R_3 = \frac{(1 + g_{cl})\psi_s}{1 - DF/2} \tag{3}$$

To return to the touchdown position of the stance phase where $\theta_1 = 90° - \psi_s/2$ and $\theta_2 = 90° + \psi_s/2$, the motor defined by θ_1 was then rotated at the slower rate (2) while θ_2 was rotated at the faster rate (3) both counterclockwise. This reset and lowered the toe to the touchdown angle position of $\psi_s/2$. This trajectory was implemented on Minitaur with a quarter time period offset between the legs and pattern of front right, hind left, front left, and hind right (FR-HL-FL-HR) based on previous studies of quadrupedal animal locomotion.[20,21]

*The singularity is the point at which both motors overlap the primary limbs which occurs at $\theta_1 = \theta_2 = 0°$ & $\theta_1 = \theta_2 = 180°$ in accordance with Fig. 2b.

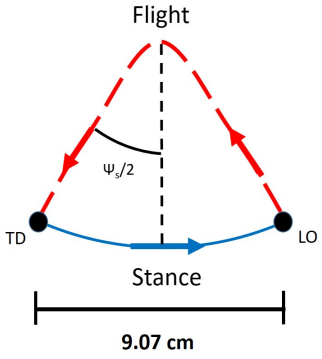

(a)

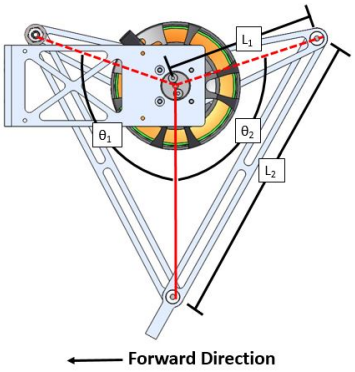

(b)

Minitaur Control Parameters	
Parameter	Value
Touch Down Angle	15°
Lift Off Angle	15°
Sweep Angle (ψ_s)	30°
Stride Length	9.07cm
Stance Height	17.32 cm
Proportional Gain	0.9
Ground Clearance (g_{cl})	1.5
Duty Factor (DF)	[75,95]%
Stride Frequency	[1.0:0.5:4.0]

(c)

Figure 2: Initial development of the leg trajectories for Minitaur. (a) Using (1), (2), (3), and the table of control parameters, the trajectory shown was produced. (b) The leg parameters are shown, where θ_1 & θ_2 are defined with respect to the vertical axis that runs from the lower joint to the center of the motors. (c) Control parameters for initial experiments with stride frequency and duty factor varied over the specified regions.

2.1 Experimental Design

Experiments were run in order to determine the control parameters that produce fast, stable walking gaits. The robot's performance was measured using a 10-camera Vicon 1.3 Motion Capture System. Plywood sheets were used as the substrate in order to provide a consistent surface as well as to increase surface friction. Minitaur was powered using a 4-cell lithium polymer battery. To reduce the impact of physical and electrical inconsistencies throughout the experiment, the order of the trials was randomized.

The initial experiments involved running the prescribed feedforward walking gait on Minitaur to evaluate overall speed and stability. For this experiment, Minitaur started at rest on one end of the plywood surface, then would run the gait once in each direction to test the viability of both directions of travel. The forward direction of travel was defined with respect to the toe extension pointing in the same direction of travel (Fig. 2b). The prescribed trajectory involved a 30° sweep angle, which results in 9.07cm stride lengths. The frequency of the leg trajectory was varied from 1 to 4 Hz in increments of 0.5 Hz. At frequencies below 1 Hz, the system did not converge to stable gaits and frequencies above 4 Hz reached a mechanical limitation due to the inertial effects of the leg. Two separate duty factors, 75% and 95%, were explored and the results of this experiment are shown in Fig. 3d & 3e.

Vicon data provided the translational positions of Minitaur in all three instantaneous degrees of freedom. Using the rate of translation in the lateral plane (parallel to the floor), the magnitude of the forward velocity was calculated. An example of this is demonstrated in Fig. 3a. This data was then filtered using a Robust Lowess Regression smoothing algorithm with a 10% span in Matlab to eliminate high frequency noise (Fig. 3b).

From this filtered velocity magnitude data, the acceleration was calculated (Fig. 3c) and used to determine the window in which Minitaur maintained a relatively consistent velocity. The algorithm locates the maximum and minimum acceleration values obtained, then uses these time points as the boundaries for the window of motion as shown in Fig. 3c. This window is then decreased by 5% to encompass only the values of velocity during which the robot was moving at or near consistent speeds (Fig. 3b). The mean value of this region was used as the velocity of the system shown in Fig. 3d & 3e.

2.2 Preliminary Experimental Analysis

The results of this set of experimental trials are summarized in Fig. 3d & 3e. It can be noted that, as expected, increasing the frequency and decreasing the duty factor resulted in increases in the overall velocity of Minitaur. Additionally, the direction of the toe extension had a surprising effect; having the toes facing opposite the direction of travel resulted in much greater speeds than when they faced the same direction. Having the feet

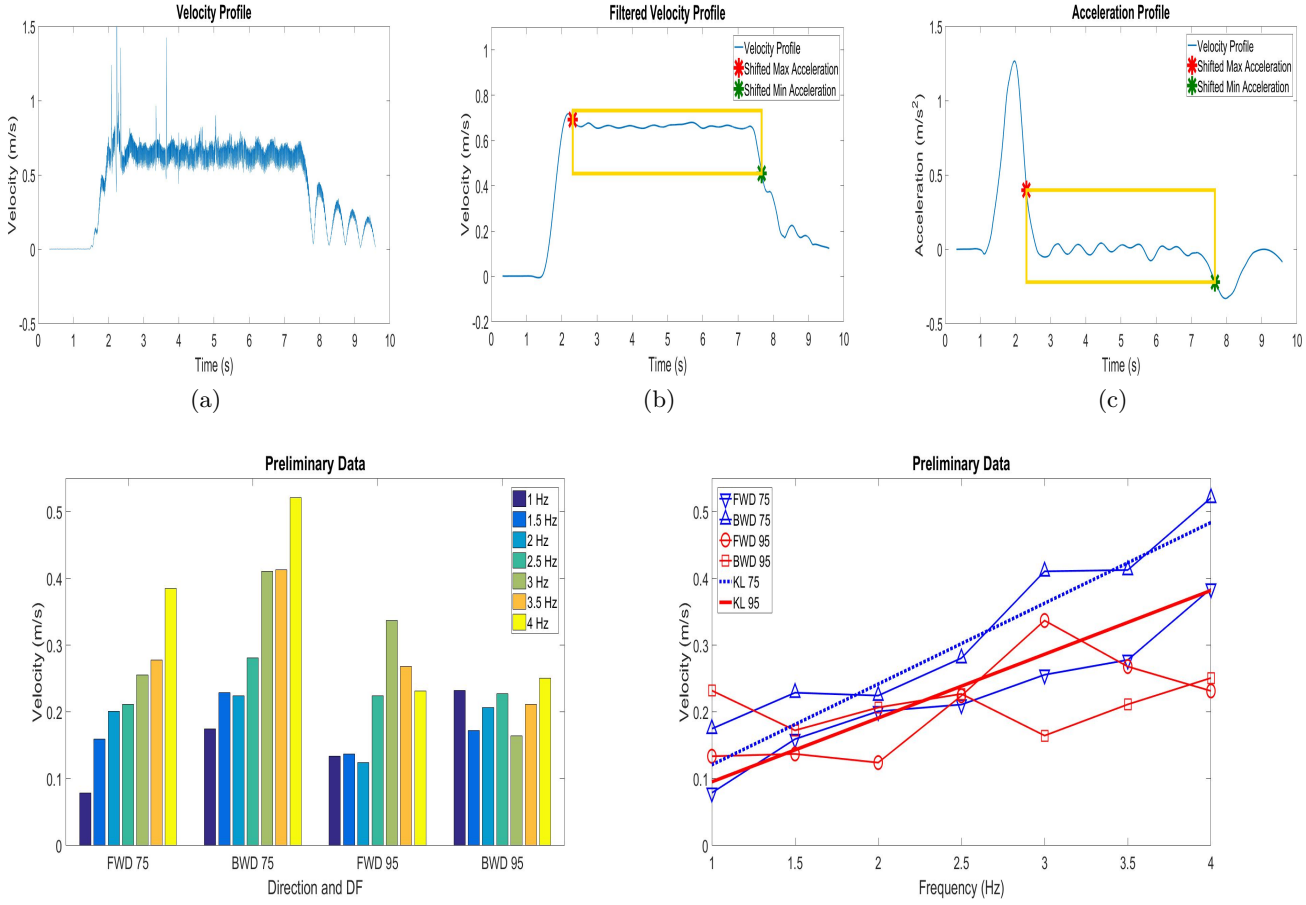

Figure 3: An example data set for determining average velocity of a run as well as the preliminary data results. (a) Velocity profiles obtained from the magnitude of the velocity of the robot in the lateral plane (parallel to the floor) from Vicon. (b) The Robust Lowess Regression Smoothing algorithm was then applied with a 10% span to filter this data. (c) The acceleration profile was produced and the maximum and minimum values were obtained. The window that these values create was then decreased by 5% and used to obtain the average velocity of the system. (d) The results of the preliminary gait analysis trials of Minitaur demonstrate the effects of changing the direction of travel, frequency, and duty factor. (e) The data is also compared to the nominally achievable values based on the kinematic limits of the system definitions.

pointed opposite the direction of travel appears to reduce the "bounce" of the feet at touchdown and aligns the foot forces favorably with the friction cones[22] resulting in a significant reduction in foot slip. As can be seen from Fig. 3d & 3e, Minitaur's maximum average velocity reached was 0.52 m/s at a frequency and duty factor of 4Hz and 75% in the backward direction of travel. Fig. 3e shows the robot's velocity as a function of stride frequency. Superimposed on these are lines representing the expected upper limit of the robot's velocity based upon stride length, frequency, and DF. This shows that in the backward foot configuration, the robot reaches expected speeds, and has effectively eliminated the detrimental effects of foot slip.

This initial gait development process also illuminated several issues with the robot's design. First of all, the instability of a few of the gait parameter sets led to significant system roll and sometimes resulted in the robot physically crashing into the ground. This led to noticeable bending of the u-brackets that support the motors for a single leg unit (Fig. 4a). Next, there were several instances in which the robot's legs heavily impacted the frame resulting in bending of the limbs of the legs (see Fig. 4b). Finally, the initial leg joints used on Minitaur

had direct contact between the aluminum links and the threading of the bolts maintaining contact of the thrust bearing/washer resulting in the wear apparent in Fig. 4c.

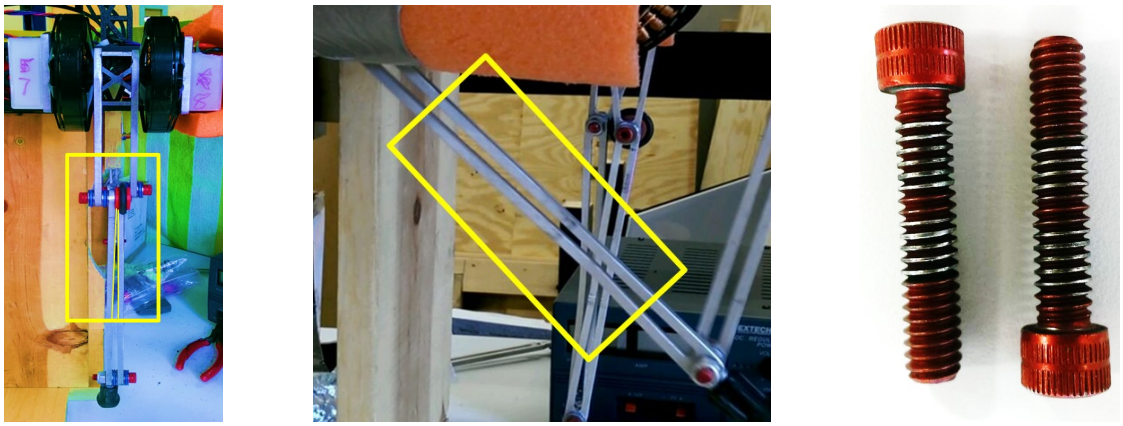

(a) (b) (c)

Figure 4: Mechanical damage to Minitaur resulting from experimentation while performing initial gait development. (a) Bending of the u-brackets resulted in noticeable inward bending and causes significant knee overlap from a frontal view of a fully extended leg ($\theta_1 = \theta_2 = 0°$). (b) Impacts of the legs with the body led to significant bending of the secondary links. (c) Direct contact between the bolts used as joints in the legs and the aluminum linkages led to visible abrasion to the bolt threadings.

3. MECHANICAL REDESIGN

To account for these mechanical failures, several modifications were implemented on the robot. As shown in Figure 5, stiffening elements were added between the motors of each leg element using thrust bearings to prevent bending of the individual u-brackets (Fig. 5a), should the robot experience a significant impact on its side either due to roll or or other dynamic impacts. This behavior resulted in a mechanical limit of the 5-bar's range of motion demonstrated in Fig. 5e. With the addition of these thrust bearings mechanical impacts will be transferred to bending the entire u-bracket. To prevent this, x-braces were fitted between adjacent legs (left & right as shown in Fig. 5b & 5f). Additionally, to minimize the impact of roll and protect the electronics of the external motor drivers, cylindrical sections of foam were fitted using laser cut ABS plastic mounts on the external surfaces of the u-brackets. This and a new ABS roll cage can be seen in Fig. 1a. To strengthen the links themselves, stiffening elements were added at their midpoint as shown in Fig. 5d & 5g. Finally, Minitaur's legs were adapted to fit a shoulder screw and bronze sleeved bearings to provide a smooth, lubricated contact (Fig. 5c,5h). Together these modifications resulted in a mass increase of 0.25 kg (4.9%), resulting in total mass of 5.40 kg for Minitaur in addition to a notable increase in the overall stiffness of the system.

In order to test the effect of these mechanical changes, a second set of experimental runs were conducted using the same experimental protocol as described in Section 2.1, resulting in the data shown in Fig. 6. From this experimental analysis, it was noted that the added stiffness and weight of the mechanical modifications resulted in failed gaits at frequencies below 2 Hz. The maximum velocity the robot achieved was 0.55 m/s, which was obtained from the toe backward direction at 3.5 Hz. This was mainly due to an increase in toe slip at the higher frequencies. For example, at 3.5Hz and a 75% duty factor, the leg slip caused the robot to complete a 90° turn during a run. The added mass and stiffness of the mechanical modifications generally led to an increase in the speed for a given gait but decreased the overall stability of these gaits, resulting in a narrowed field of successful stride frequencies.

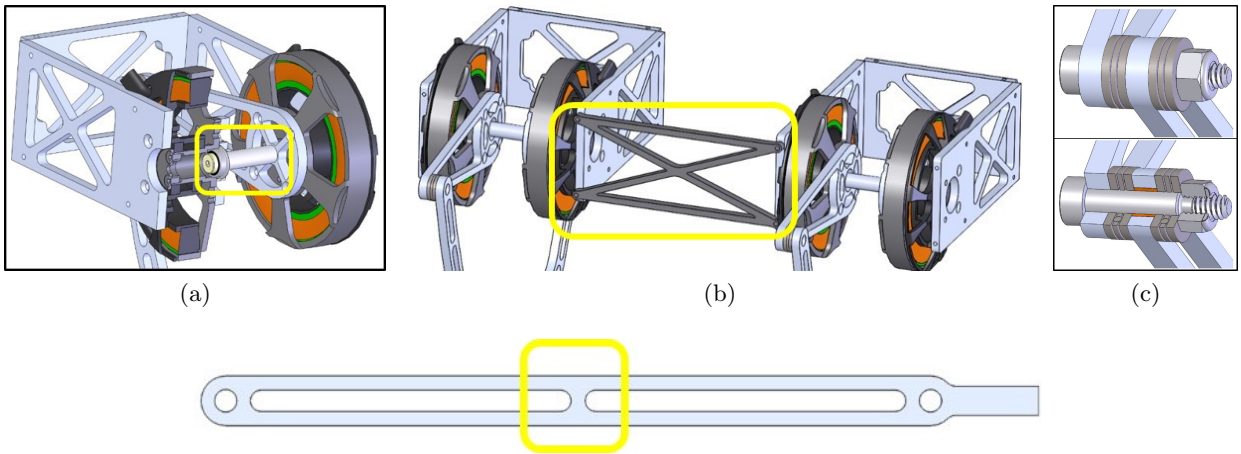

(a) (b) (c)

(d)

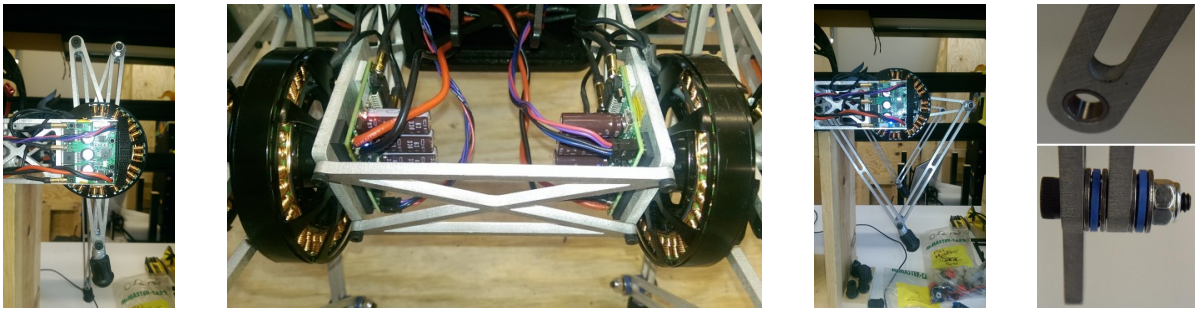

(e) (f) (g) (h)

Figure 5: Damage to Minitaur during initial experimentation motivated mechanical adjustments to the robot's physical structure. (a) CAD drawings of the thrust bearing mounts designed to prevent bending of the u-brackets from collisions, (b) x-braces placed between each leg to prevent the overall bending of the u-brackets, (c) design of the new bearings for smoother joint rotations, and (d) modified leg elements with a bracing element inserted in the center. (e) Addition of the stiffening thrust bearings between motors of a leg results in a limitation on the workspace for the legs of Minitaur. (f) The x-braces also provided a secondary form of protection for the motor drivers on the inner motors. (g) The stiffening elements added to the leg segments to help prevent bending of the links. (h) The new bearings provided smoother joints for Minitaur's legs.

4. CONTROL MODIFICATIONS

To improve upon the initial method for gait development, several aspects of the control scheme were modified. First a method for mapping the forward kinematics was implemented in order to allow direct manipulation of the shape of the toe trajectory. The shape of this toe trajectory was then explored with the aim of obtaining fast, stable walking gaits.

4.1 Translating Between Motor Space & End Effector Space

Working in the joint (motor) space has several limitations, particularly regarding the construction of linear motions (with the exception of leg extension radially out from the motor centers). For this reason, the inverse kinematics were derived to perform real time calcuations based off of set waypoints of Cartesian coordinates defined in the end effector space. Due to the symmetric nature of the 5-bar linkage used on Minitaur, the inverse kinematics can be simplified as a two bar linkage centered along the legs axis of symmetry (see Fig. 7). Therefore, from a given x and y value within the workspace, the total length from hip to toe can be calculated as $L = \sqrt{x^2 + y^2}$. With this value obtained, the inner angle of rotation of the leg from vertical orientation can be calculated as:

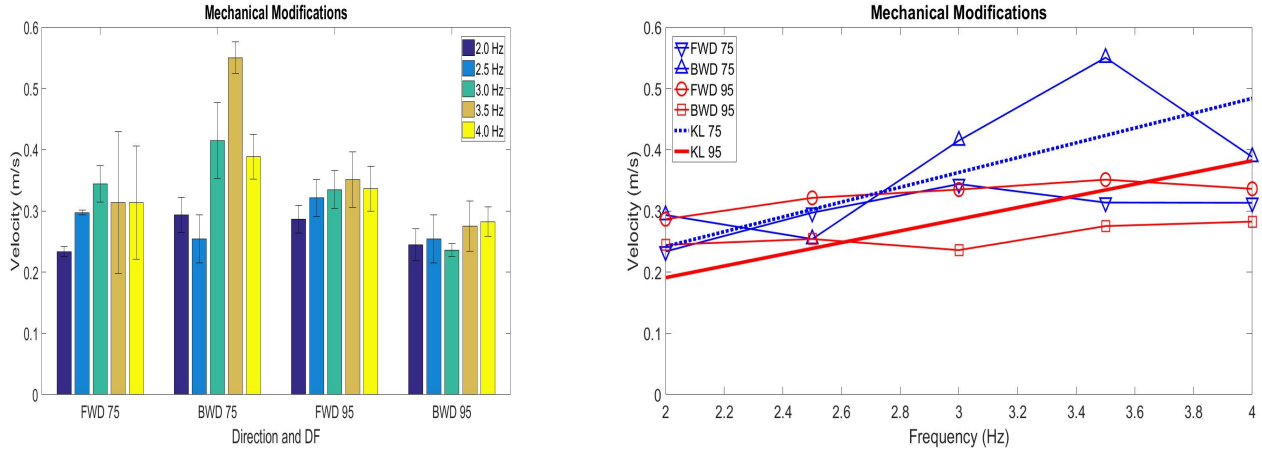

(a) (b)

Figure 6: After the mechanical modifications were implemented a sweep of the frequency from 2-4 Hz in increments of 0.5 Hz and duty factors of both 75% and 95% were performed as was done in Section 2.2. Each of these sets of parameters were run in three trials with randomized order. (a) The average velocities produced after the mechanical changes were implemented. (b) The resulting velocities were generally higher than before for gaits that were stable and smooth (2-3.5 Hz).

$$\psi = asin(x/L) \tag{4}$$

The angle of the leg itself with respect to this rotated frame of reference can then be calculated using law of cosines as:

$$\phi = acos\left[\frac{L_1^2 + L^2 - L_2^2}{2L_1 L}\right] \tag{5}$$

From (4) & (5), the control angles of the motors are then defined as $\theta_1 = \phi - \psi$ and $\theta_2 = \phi + \psi$.

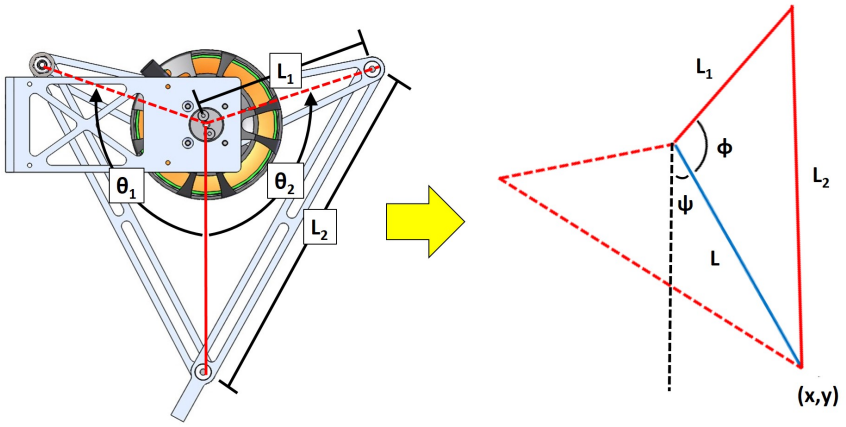

j jv jhjbjj ng

Figure 7: The end effector space is defined by the position of the end effector in (x, y) coordinates with respect to the motors. To determine the motor positions required to produce the desired location in the two dimensional space, the values of ψ & ϕ were calculated as demonstrated in (4) & (5) respectively.

4.2 Trajectory Shaping

Switching to an end effector based control allowed for much greater freedom in modifying the overall toe trajectory. The initial trajectory was adapted from joint space to an isosceles triangular trajectory as shown in Fig. 8a. From this base trajectory, the location of the toe apex (top of the triangle) was manipulated laterally (Fig. 8b) and the overall walking height (Fig. 8a) were adjusted. The goal of this is to see whether faster gaits can be generated from toe trajectories where the toe touchdown occurs at or near body velocity (akin to ground speed matching[23]) and by using animal-like foot trajectory shapes.[10] In addition to these changes the sweep angle was increased, increasing the lateral distance from 9 to 12 cm during stance. The effects of this trajectory shaping were then experimentally evaluated through a set of runs with these parameters at 3 Hz and a 75% duty factor. This set of parameters was chosen because they provided the most stable and consistent velocities in the experiments described in Section 3.

With this new control policy a set of experimental trials were run with varying the stance height and apex lateral location. Figure 8c shows the resulting robot speeds. From which, it can be seen that when the stance height is maintained at the nominal position ($\theta_1 = \theta_2 = 90°$), the peak speeds were achieved with the right and obtuse triangle configurations. This resulted in velocities much greater than those of the motor space-based trajectory. The minimization of foot slipping and added effects of forward bounce using the obtuse leg trajectory in the backwards running direction appears to result in ground speed matching that helps the robot achieve speeds up to 0.92 m/s.

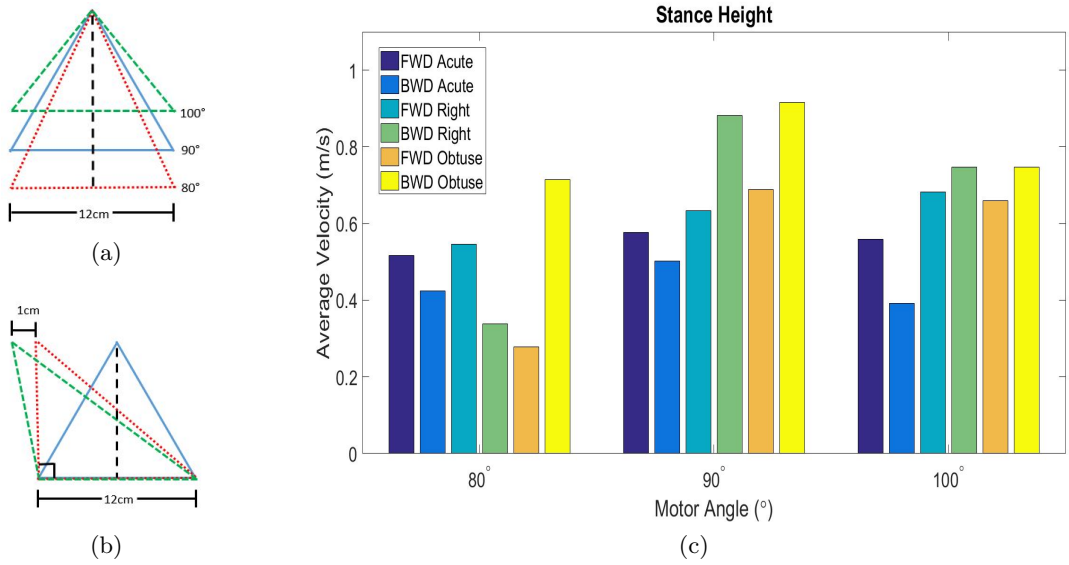

Figure 8: To improve the walking gait, manipulations of the trajectory were implemented based on the end effector space. (a) The stance height was varied, by adjusting the motor angles at stance to 80°, 90°, and 100°. (b) The apex of the triangle was adjusted to evaluate the difference between an acute isosceles triangle (matching the previous trajectory), a right triangle, and an obtuse triangle. (c) These trials were run at a 3Hz frequency and a DF of 75%, with one trial of each combination in a randomized order.

4.3 Trotting

The identification of gait parameter settings that produce smooth, reliably fast walking gaits, motivated attempts at faster motions with the implementation of a trotting gait. For a trot, the front right and back left legs move as a synchronous pair while the front left and back right act together. These leg sets are activated with a half time period offset in between. Since the duty factor of a trotting gait is 50, the flight phase has a longer amount of the time period which allows a greater degree of accuracy in matching of the actual toe position to the prescribed trajectory. Therefore, this trotting gait was run at 4.5 Hz (slightly faster than the walking gaits)

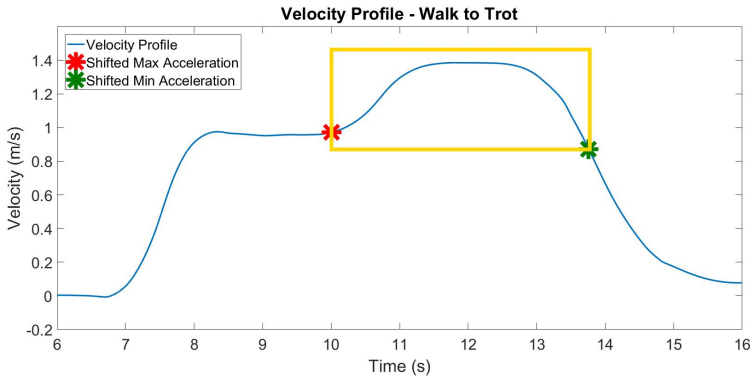

(a)

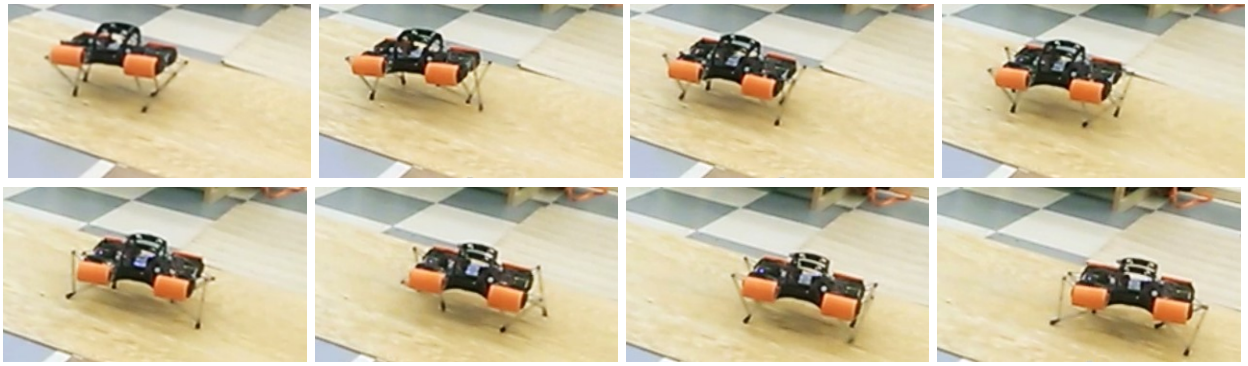

(b)

Figure 9: Analysis of Minitaur trotting gaits with obtuse triangular trajectories. (a) FIltered Walk-to-trot funneling data (described in Section 2.2) for the forward direction, obtuse triangular trajectory (walk @3.5 Hz, trot @4.5 Hz). (b) Time lapsed photos of Minitaur trotting on plywood.

and with the asymmetric triangle at normal stance height (both motors at 90°; $\theta_1 = \theta_2 = 90°$). These trotting gaits were preceded by a walking gait of 3.5 Hz to perform velocity funneling. An average maximum velocity of 1.33 ($\pm$0.087) m/s was achieved under these conditions and this trotting gait demonstrated stable, steady state behavior (Fig. 9a). This speed is nearly three times that of the initial gaits developed on the less mechanically robust platform.

5. OBSTACLE DETECTION AND CLEARANCE

The development of a set of stable and fast walking and trotting gaits enables the next step, developing techniques for obstacle detection and clearance. One of the most consistent, man-made obstacles encountered in the real world are stairs so we began with developing stair climbing gaits. The first approach involved the direct manipulation of the trajectory to match the dimensions of the stairs. This method failed due to the excessive load experienced on the back legs leading to significant pitching and rolling of the robot. The next approach involved rotating the trajectory of the previously described feedforward gait to compensate for the slope of the stairs.[15] This was done by adjusting the stance of the robot to maintain the robots body parallel to the slope of the stairs as shown in Fig. 10. This new baseline for stance was then used to as the central base of the triangular trajectory, with the entire triangle rotated so that this base was parallel with the slope of the stairs as well. Despite some initial success with this approach when the robot was placed on the stairs, the robot is unable to identify when stairs are encountered or to transition from a walking or running gait to a stair climbing gait. In order to enable more robust gaits and these types of behavior transitions, we investigate a method for accurate sensing of contact forces at the feet.

In general, force sensing at the feet can help locomotion in several important ways. It can, as suggested above, be used as a contact sensing mechanism to trigger specialized behaviors such as stair climbing. It can also serve to estimate the stance period of a gait, or help in determining leg slippage and in activating traction control schemes. In addition, by properly estimating ground reaction forces, it would be possible to perform gait adaptation to balance leg loading and/or modulate limb stiffness.

Initial attempts to implement foot sensing used the encoder to compare the error in trot trajectory location and velocity. A threshold was set for this error in order to determine when collision with an obstacle occurred. Unfortunately, this method only worked a fraction of the time since the threshold of the error was either too large which would result in the dynamics of walking and ground reaction forces triggering contact sensation, or too small, preventing the detection of obstructions.

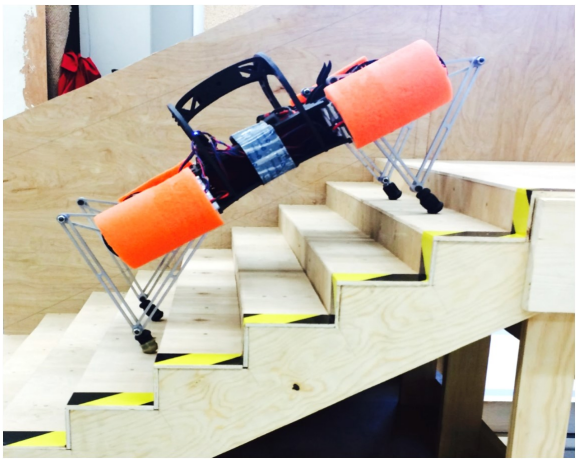

Figure 10: Minitaur with a rotated stance demonstrating the slope compensation for initial attempts at developing stair climbing gaits.

5.1 Leg Proprioception

Fortunately, the legs in the Minitaur are rigid and are directly driven by two Brushless DC motors. Therefore, by developing the leg Jacobian and measuring the currents through the motor phases, joint torques can be mapped into ground-leg reaction forces. This should greatly improve the force sensing accuracy for obstacle detection and gait adaptation techniques.

Following Fig. 11, the leg Jacobian can be computed as follows

$$\beta = q_2 - q_1, \tag{6}$$

$$X = l_1 \cos q_1 + l_2 \cos \delta, \;\; Y = l_1 \sin q_1 + l_2 \sin \delta, \tag{7}$$

where

$$\cos \delta = -\cos\left(q_1 - \arccos\sqrt{\frac{1-\cos\beta}{2}} - \arccos\left(\frac{l_1}{l_2}\sqrt{\frac{1-\cos\beta}{2}}\right)\right), \tag{8}$$

$$\sin \delta = -\sin\left(q_1 - \arccos\sqrt{\frac{1-\cos\beta}{2}} - \arccos\left(\frac{l_1}{l_2}\sqrt{\frac{1-\cos\beta}{2}}\right)\right). \tag{9}$$

Taking time derivatives of X and Y, it is then possible to write the leg Jacobian J as follows

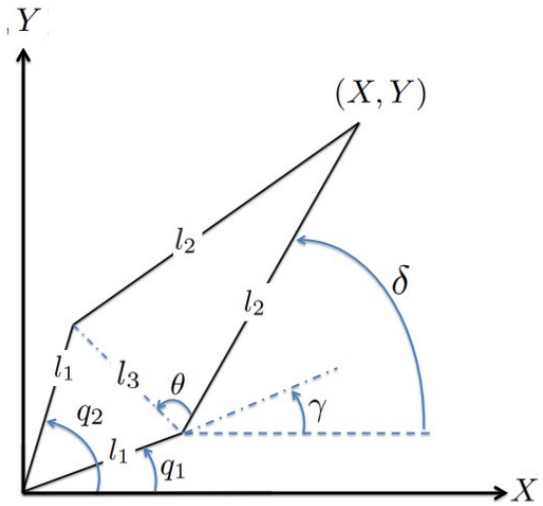

Figure 11: Parameter definitions for a single Minitaur with generalized coordinates q_1 and q_2 in order to determine the Jacobian of the 5-bar mechanism.

$$\begin{bmatrix}\dot{X}\\ \dot{Y}\end{bmatrix} = \begin{bmatrix}-l_1\sin q_1 - l_2(1-(A+D))\sin\delta & -l_2(A+D)\sin\delta\\ l_1\cos(q_1) + l_2(1-(A+D))\cos\delta & l_2(A+D)\cos\delta\end{bmatrix}\begin{bmatrix}\dot{q_1}\\ \dot{q_2}\end{bmatrix} = J\begin{bmatrix}\dot{q_1}\\ \dot{q_2}\end{bmatrix}, \tag{10}$$

where $A = \frac{1}{2\sin\beta}$ and $D = \frac{l_1}{2l_2\sqrt{2}}\frac{1}{\sqrt{1-\cos\beta}}\frac{1}{\sqrt{1-\frac{l_1}{l_2}\frac{1-\cos\beta}{2}}}$.

It is important to recall that the leg Jacobian can also be used to map end effector (foot) forces to joint torques (τ_1 and τ_2) as follows

$$\begin{bmatrix}\tau_1\\ \tau_2\end{bmatrix} = J^T\begin{bmatrix}F_X\\ F_Y\end{bmatrix} \tag{11}$$

In order to use (11) to predict ground reaction forces, it is necessary to estimate joint torques. As mentioned in Section 1, the Minitaur legs are equipped with two Brushless DC motors. These motors are connected in a Y electrical configuration and utilize field control with sinusoidal commutation. As illustrated in Fig. 12, this type of control scheme attempts to maintain the generated stator current vector perpendicular to the rotor (i.e., along the q axis). By doing so, the generated torque is maximized. In order to achieve this, the currents through each of the phases are shifted by 120° from the other two. That is:

$$IA = I\sin(\theta), IB = I\sin(\theta+120), IC = I\sin(\theta+240), \tag{12}$$

where θ represents the rotor position.

Since the windings are physically oriented 120° from each other, the net current along the X and Y axis of the stator can be computed as:

$$IX = IA\cos(90) + IB\cos(90+120) + IC\cos(90+240) \tag{13}$$
$$IY = IA\sin(90) + IB\sin(90+120) + IC\sin(90+240) \tag{14}$$

Therefore, the net magnitude of the stator current is

$$I_{net} = \sqrt{IX^2 + IY^2} = 1.5I. \tag{15}$$

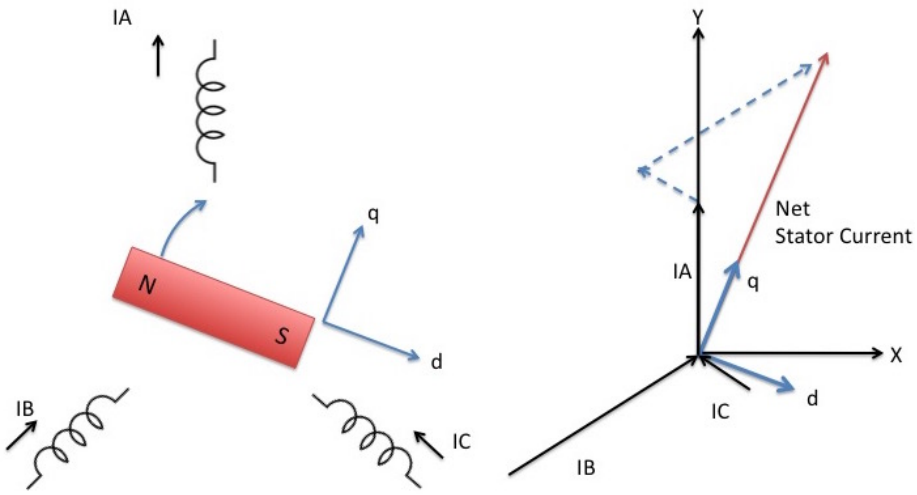

Figure 12: For maximum torque output, sinusoidal commutation with the field control attempts to maintain the stator current vector perpendicular to rotor.

Keeping in mind that Brushless-DC motors are essentially linear actuators, one can estimate the produced motor torque as

$$\tau = K_t I_{net} \tag{16}$$

where K_t is the motor torque constant.

5.1.1 Experimental Setup and Preliminary Results

In order to validate the proposed approach to estimate ground reaction forces, the single leg setup shown in Fig. 13 was constructed. The setup has a six-axis Gamma ATI force plate at the bottom and is also equipped with three ACS709 sensors to monitor the current through each phase of the motor. In particular, we measure the currents IA, IB, and IC, and then use (13)-(16) to estimate the motor torque. The current sensors are connected to 12-bit A/D channels of the National Instruments myRIO board. Motor joint positions are collected by the Minitaur main controller board and then sent via serial communication to the myRIO.

The preliminary experiments conducted in this work consisted in a set of trials where the leg was commanded to push down in the normal direction to the plate. As shown in Fig. 14a, five different experiments were performed by varying the commanded joint angles q_1 and q_2. By varying the angles in this fashion, we are effectively commanding the foot to reach different depths into the force plate. Since Minitaur relies in PD control laws to track the commanded foot position, each experiment from 1 through 5 results in an increased position error and therefore a larger applied downward force.

Figure 14b, compares results obtained via current measurement against force plate measurements. With the exception of experiment 1, the estimation errors are below 7%. Although the errors are small, there are at least two deficiencies that will be remediated in future work: First, the foot of Minitaur is slightly offset from the joint connecting the links labeled l_2 in Fig. 11. This offset should be considered in the leg Jacobian. Second, the single leg electronics only monitors currents through one of the motors and assumes that the current through the second one is the same. Once these two limitations are solved, we will continue with the validation of the force sensing approach using leg configurations where lateral forces are also relevant. In addition, we will start studying force sensing under dynamic conditions.

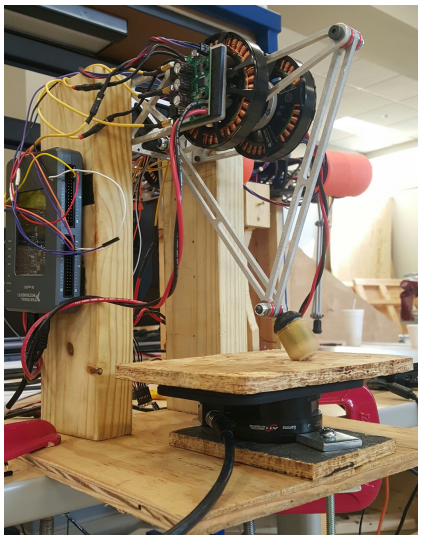

Figure 13: The experimental single leg setup designed to validate the estimation of ground-leg reaction forces based on current readings and force plate measurements.

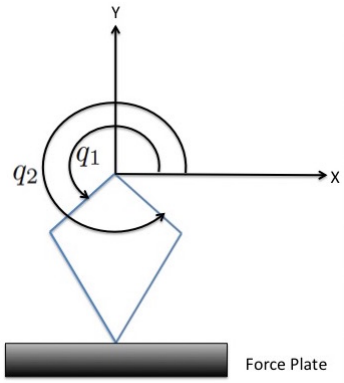

Exp	$q_{1\,com}$ [rad]	$q_{2\,com}$ [rad]	Depth Into Plate[cm]
1	2.2π/2	3.8π/2	2.27
2	2.3π/2	3.7π/2	4.03
3	2.4π/2	3.6π/2	5.76
4	2.5π/2	3.5π/2	7.37
5	2.6π/2	3.4π/2	8.80

(a)

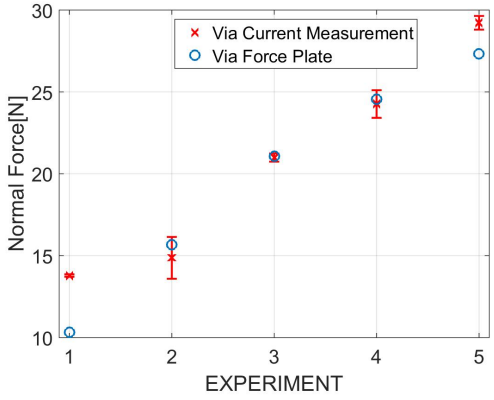

(b)

Figure 14: Experimental results comparing force plate measurements collected from commanding the 5-bar leg to the angles defined against estimation of normal force via current measurement. Each experiment comprises 5 runs.

6. CONCLUSIONS

In this paper, an initial walking gait was designed using the motor space of the 5-bar leg mechanisms utilized by Minitaur. This clock-based, feedforward trajectory was then implemented on the quadrupedal robot and analyzed for system speed and stability. The system achieved a maximum velocity of 0.52 m/s and closely followed the kinematic predictions, providing a good indication that the gait developed did not produce significant foot slip. Mechanical modifications were then implemented to increase the mechanical robustness and rigidity of the system. The same gait was implemented on this system and resulted in a maximum velocity of 0.55 m/s. Though the range of frequencies and duty factors resulting in successful gaits was narrowed, the overall robustness of the robot increased.

The walking gait was then modified to allow a manipulation of the trajectory shape via the selection of way points within the foot workspace with the aim to emulate animal-like leg trajectories. This method was used

to implement different walking heights as well as slight variation in the geometry of the triangular trajectory shape chosen. Refinement of the trajectory shape led to the increase in velocity to 0.92 m/s, demonstrating an improvement in the walking gait of Minitaur. To expand upon this result further, the trajectory chosen was implemented with a trotting gait utilizing the principles of gait funneling to evaluate the animal-like running of the system and produce faster locomotion. A maximum velocity of 1.33 ($\pm$0.087) m/s resulted from these tests with stable, steady state behavior (Fig. 9a).

Several methods were explored towards the development of stair climbing gait development as well as sensing, though initial tests were unsuccessful. As a first step to refining gait development and enabling obstacle detection and clearance moving forward, work began towards incorporating contact sensing. A study on the estimation of ground-leg reaction forces via the leg Jacobian and current sensing was performed with using current sensors and a force plate. Preliminary results with a single leg setup showed good prediction of foot forces. Encouraged by these findings, future work will transition the force sensing methodology to Minitaur to enable testing under dynamic conditions. Force sensing in the robot will be crucial in the development of gaits and control approaches that favor leg loading and follow desired force profiles. Furthermore, force sensing will help with the detection and traversal of obstacles such as stairs.

ACKNOWLEDGMENTS

This work was supported by the collaborative participation in the Robotics Consortium sponsored by the U.S. Army Research Laboratory under the Collaborative Technology Alliance Program, Cooperative Agreement DAAD 19-01-2-0012. The U.S. Government is authorized to reproduce and distribute reprints for Government purposes not withstanding any copyright notation thereon. Thanks to Charles Young and Tyler Jonas for their help with the design and implementation of the mechanical modifications to Minitaur.

REFERENCES

[1] Raibert, M., Blankespoor, K., Nelson, G., Playter, R., et al., "Bigdog, the rough-terrain quadruped robot," in [*Proceedings of the 17th World Congress*], **17**(1), 10822–10825 (2008).

[2] Kimura, H., Fukuoka, Y., and Cohen, A. H., "Adaptive dynamic walking of a quadruped robot on natural ground based on biological concepts," *The International Journal of Robotics Research* **26**(5), 475–490 (2007).

[3] Altendorfer, R., Moore, N., Komsuoglu, H., Buehler, M., Brown Jr, H. B., McMordie, D., Saranli, U., Full, R., and Koditschek, D. E., "Rhex: a biologically inspired hexapod runner," *Autonomous Robots* **11**(3), 207–213 (2001).

[4] Tsujita, K., Tsuchiya, K., and Onat, A., "Adaptive gait pattern control of a quadruped locomotion robot," in [*Intelligent Robots and Systems, 2001. Proceedings. 2001 IEEE/RSJ International Conference on*], **4**, 2318–2325, IEEE (2001).

[5] Billard, A. and Ijspeert, A. J., "Biologically inspired neural controllers for motor control in a quadruped robot," in [*Neural Networks, 2000. IJCNN 2000, Proceedings of the IEEE-INNS-ENNS International Joint Conference on*], **6**, 637–641, IEEE (2000).

[6] Kajita, S. and Tani, K., "Adaptive gait control of a biped robot based on realtime sensing of the ground profile," in [*Robotics and Automation, 1996. Proceedings., 1996 IEEE International Conference on*], **1**, 570–577, IEEE (1996).

[7] Wang, X., Li, M., Wang, P., Guo, W., and Sun, L., "Bio-inspired controller for a robot cheetah with a neural mechanism controlling leg muscles," *Journal of Bionic Engineering* **9**(3), 282–293 (2012).

[8] Seipel, J. and Holmes, P., "A simple model for clock-actuated legged locomotion," *Regular and chaotic dynamics* **12**(5), 502–520 (2007).

[9] Saranli, U., Buehler, M., and Koditschek, D. E., "Design, modeling and preliminary control of a compliant hexapod robot," in [*Robotics and Automation, 2000. Proceedings. ICRA'00. IEEE International Conference on*], **3**, 2589–2596, IEEE (2000).

[10] Moro, F. L., Spröwitz, A., Tuleu, A., Vespignani, M., Tsagarakis, N. G., Ijspeert, A. J., and Caldwell, D. G., "Horse-like walking, trotting, and galloping derived from kinematic motion primitives (kmps) and their application to walk/trot transitions in a compliant quadruped robot," *Biological cybernetics* **107**(3), 309–320 (2013).

[11] Kim, M. S. and Uther, W., "Automatic gait optimisation for quadruped robots," in [*Australasian Conference on Robotics and Automation*], 1–3, Citeseer (2003).

[12] Fukuoka, Y., Habu, Y., and Fukui, T., "A simple rule for quadrupedal gait generation determined by leg loading feedback: a modeling study," *Scientific reports* **5** (2015).

[13] Juang, J.-G., "Fuzzy neural network approaches for robotic gait synthesis," *Systems, Man, and Cybernetics, Part B: Cybernetics, IEEE Transactions on* **30**(4), 594–601 (2000).

[14] Ijspeert, A. J., "Central pattern generators for locomotion control in animals and robots: a review," *Neural Networks* **21**(4), 642–653 (2008).

[15] Gehring, C., Bellicoso, C. D., Coros, S., Bloesch, M., Fankhauser, P., Hutter, M., and Siegwart, R., "Dynamic trotting on slopes for quadrupedal robots," in [*Intelligent Robots and Systems (IROS), 2015 IEEE/RSJ International Conference on*], 5129–5135, IEEE (2015).

[16] Moore, E., Campbell, D., Grimminger, F., and Buehler, M., "Reliable stair climbing in the simple hexapod'rhex'," in [*Robotics and Automation, 2002. Proceedings. ICRA'02. IEEE International Conference on*], **3**, 2222–2227, IEEE (2002).

[17] Kenneally, G., De, A., and Koditschek, D., "Design principles for a family of direct-drive legged robots," in [*Robotics Science and Systems Workshop on Miniature Legged Robots*], (2015).

[18] Seok, S., Wang, A., Otten, D., and Kim, S., "Actuator design for high force proprioceptive control in fast legged locomotion," in [*Intelligent Robots and Systems (IROS), 2012 IEEE/RSJ International Conference on*], 1970–1975, IEEE (2012).

[19] Kim, S., Clark, J. E., and Cutkosky, M. R., "isprawl: Autonomy, and the effects of power transmission," in [*Climbing and Walking Robots*], 859–867, Springer (2005).

[20] Schöner, G., Jiang, W. Y., and Kelso, J. S., "A synergetic theory of quadrupedal gaits and gait transitions," *Journal of theoretical Biology* **142**(3), 359–391 (1990).

[21] Hildebrand, M., "Symmetrical gaits of primates," *American Journal of Physical Anthropology* **26**(2), 119–130 (1967).

[22] Abate, A., Hatton, R. L., and Hurst, J., "Passive-dynamic leg design for agile robots," in [*Robotics and Automation (ICRA), 2015 IEEE International Conference on*], 4519–4524, IEEE (2015).

[23] Hodgins, J. K. and Wooten, W. L., [*Animating human athletes*], Springer (1998).